# MINISTRY OF EDUCATION
## Academic Research Fund (AcRF) Tier 1 – Final Report

**Name of Institute / Department**

Department of Electrical and Computer Engineering, Faculty of Engineering, National University of Singapore

**Discipline Cluster**

Physics and Engineering (EP5)

**Name of PI**

Jimmy Chih-Hsien PENG

**Project Title**

A Comprehensive Design of Community Microgrid

**Grant information**

| | |
|---|---|
| Approved Budget | $150,527.00 |
| WBS Number | R-263-000-D10-114 |
| Start & End Date | 01/03/2018 to 28/02/2021 |

**1. Short Summary of the Project**

This project presents a comprehensive design of a hybrid AC/DC microgrid to enable the smooth transition of the community grid to a “smart” and sustainable future. We conceptualized the topology of such a microgrid and developed resilient control strategies for ensuring plug-and-play of renewables, storage, and loads. In tandem, we developed a novel energy management system for optimally scheduling the flexible loads in the system with a view to minimize the total electricity cost, while maximizing consumer participation in such ancillary services. We also considered the stability and resilience implications of AC/DC and DC/DC converters interacting amongst each other in such systems. We developed novel microgrid models that have reduced computational complexity, nevertheless retaining accuracy. Subsequently, we proposed controller designs that can guarantee the stability for a wide range of operating conditions. These designs were evaluated using numerical simulations and hardware experiments.

**2. Underpinning Research**

Decarbonization through renewable generation integration and introduction of prosumer-oriented ancillary services help to fight against climate change and improve the grid efficiency. Nevertheless, such intermittent generation, consumer variability, adoption of smarter home appliances and Electric Vehicles, etc. introduce uncertainties for the grid operation and security, while also providing an opportunity for improving the grid performance and resilience. To this end, this project has developed stability theory, modelling tools, and control methods to support future grid management, particularly for community microgrids—the future trend of residential grids.

The following presents a summary of the various researchers involved in this project and their contributions.

- Gurupraanesh RAMAN (Research Scholar from Mar. 2018—July 2020) investigated hybrid AC/DC topologies for community microgrids. He focused on deriving numerical models and simulations of such microgrids and developed decentralized control schemes. Subsequently, he investigated stability within and between multiple microgrids, and developed a hardware testbed

for validating the theoretical models. The latter also involved developing efficient power electronic converters.

- Gururaghav RAMAN (Research Scholar from Mar. 2018—May 2020 and Research Fellow from Aug. 2020—Feb. 2021) also contributed to the above-mentioned research on microgrid topologies and control. Importantly, his research was focused on the community acceptance and behavioural aspects of the project. His study developed realistic bottom-up load profile models, implemented residential demand response for home appliances and residential electric vehicles (EVs), and developed an optimal energy management system for such microgrids.

- Andrey GORBUNOV (Research Scholar from Aug. 2018—Feb. 2021) studied oscillations in multi-microgrid systems, specifically on analysing the dependence and sensitivity of such oscillations on the interconnection topology using graph-theoretical concepts.

- Subham SAHOO (Research Fellow from Apr. 2018—Apr. 2019) investigated the resilience of such microgrids, focusing on data corruption and malicious attacks on such microgrids. His study resulted in the development of attack detection, identification, and mitigation in real-time.

- Jingqiu ZHANG (Research Scholar from Jan. 2019—Feb. 2021) contributed towards the research on microgrid resilience, focusing on false data injection attacks.

- John Long SOON (Research Fellow from Apr. 2019—June 2020) worked on developing efficient power electronic converters for the DC-side of the community microgrids. Specifically, the efficiency improvement was reached by preventing saturation in the inductor using a wide range of techniques such as AC and DC biasing.

## 3. Summary of Project Findings

**Microgrid topology and differential-droop control**

We have developed a transitional microgrid topology for residential buildings. This hybrid AC/DC microgrid forms an intermediate stage in the transition from AC to pure DC residential power distribution. This topology is shown in Fig. 1.

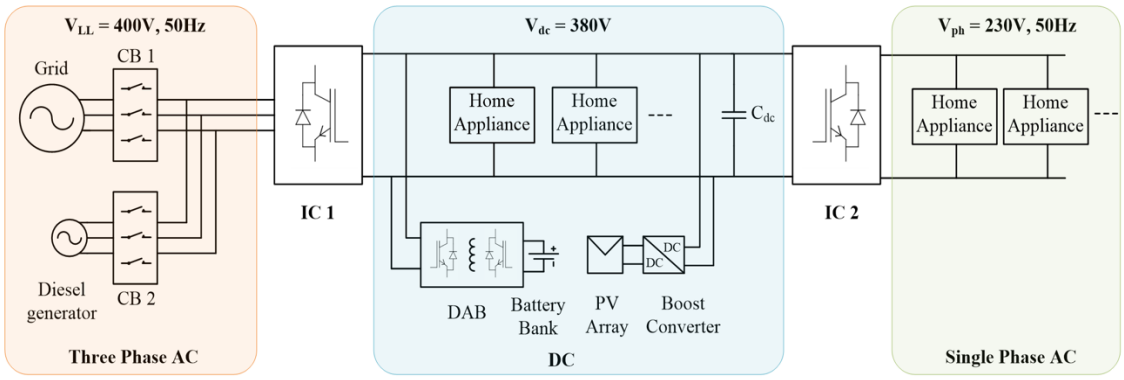


**Fig. 1. Proposed transitional residential microgrid topology.**

This microgrid design consists of a 380V DC subgrid, and a 230 V single-phase AC section, which can supply both DC and AC loads in the building. The power flow between the main power grid and the two subgrids is controlled by two interlinking converters IC1 and IC2. Under grid-connected operation, IC1 behaves as a rectifier, setting a constant voltage of 380V at the DC bus, and IC2 in turn maintains the AC voltage at 230V. However, under islanded operation, IC1 shares the total load among the battery energy storage system (BESS), PV array, and the diesel generator.

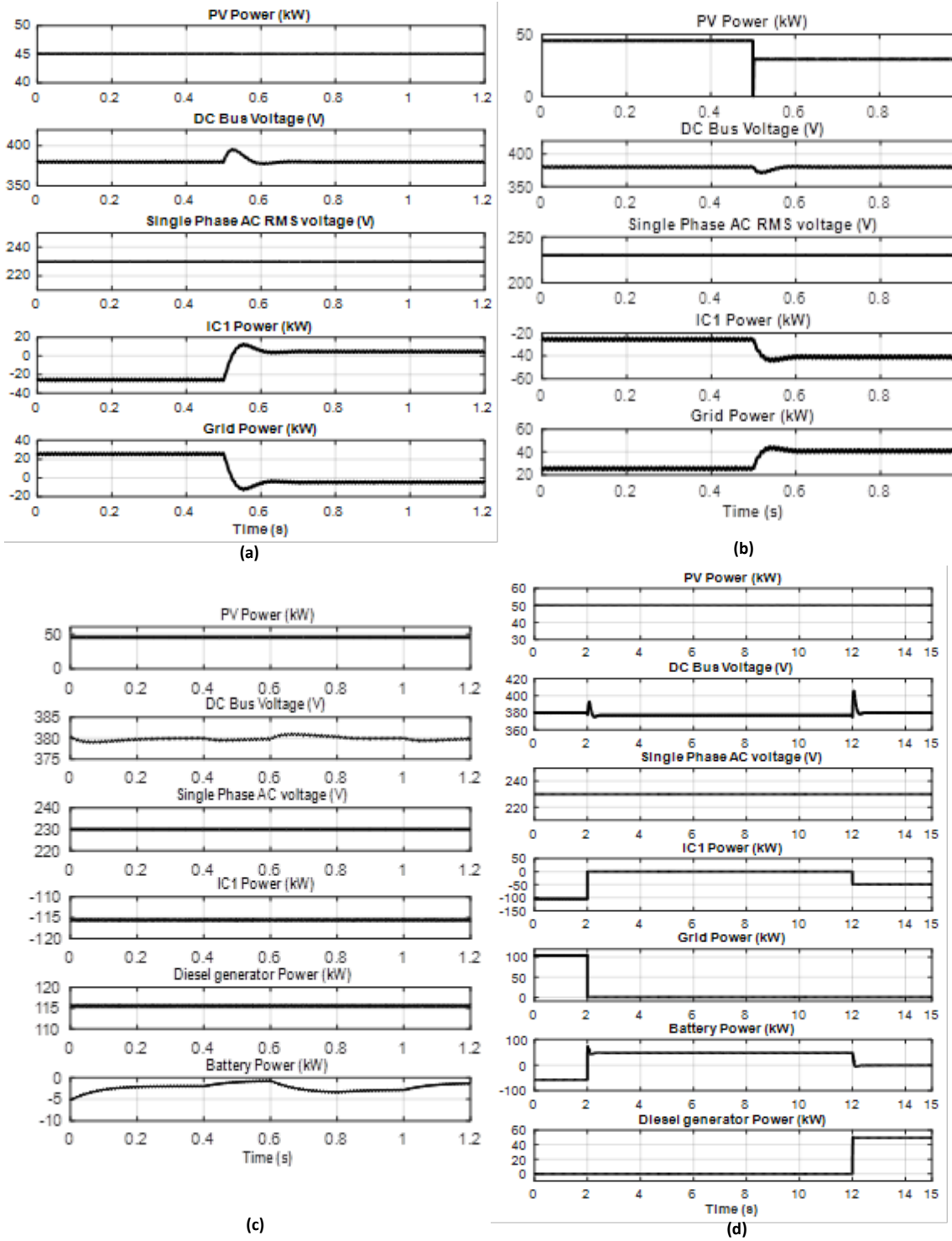


**Fig. 2. (a) Plots of the residential microgrid when subjected to a load change (50kW to 20kW) and constant PV generation under grid-connected mode, (b) system response to variations in PV generation for a constant load under grid-connected mode, (c) simulated results of random load variations (±1% about the rated load) under islanded mode, and (d) transition from grid-connected to islanded mode.**

The power sharing equations in this scenario are as follows:

$$V_{dc} = \tilde{V}_{dc} - k_{dc}P_{BESS} \quad (1)$$

where $\tilde{V}_{dc}$ is the nominal value of the DC bus voltage (380V), $k_{dc}$ is the droop coefficient, and $P_{BESS}$ is the power drawn from the battery storage. Now, the DC bus voltage is used as an indicator for the power deficit/surplus in the building. The power reference for IC1 is then defined as:

$$P_{IC1} = \frac{1}{k_{IC}}\left(V_{dc} - \tilde{V}_{dc}\right) \quad (2)$$

where $k_{IC}$ is the droop constant of IC1.
The proposed control strategy is implemented for a typical 10-storey residential apartment, where each level comprises of three units. Simulation results shown in Fig. 2 illustrate the merits of the proposed architecture and control strategy. These results assume a 4% drop in the voltage output of the battery with respect to its power rating, and therefore $k_{dc}$=6.09E-5 V/W. We further assume that 5% of the IC1 charges the battery while the remaining diesel generation supplies the load. Therefore, $k_{dc}/k_{IC}$=1.05, and subsequently $k_{IC}$=5.79E-5 V/W. It is clear from these scenarios that the DC and AC bus voltages remain stable under irradiance and load changes, as well as during the transition between the grid-connected and islanded modes.

**Demand response implementation**

Demand response and building energy management is implemented in the transitional topology as shown in Fig. 3. In this case, the entire building behaves as a virtual power plant.

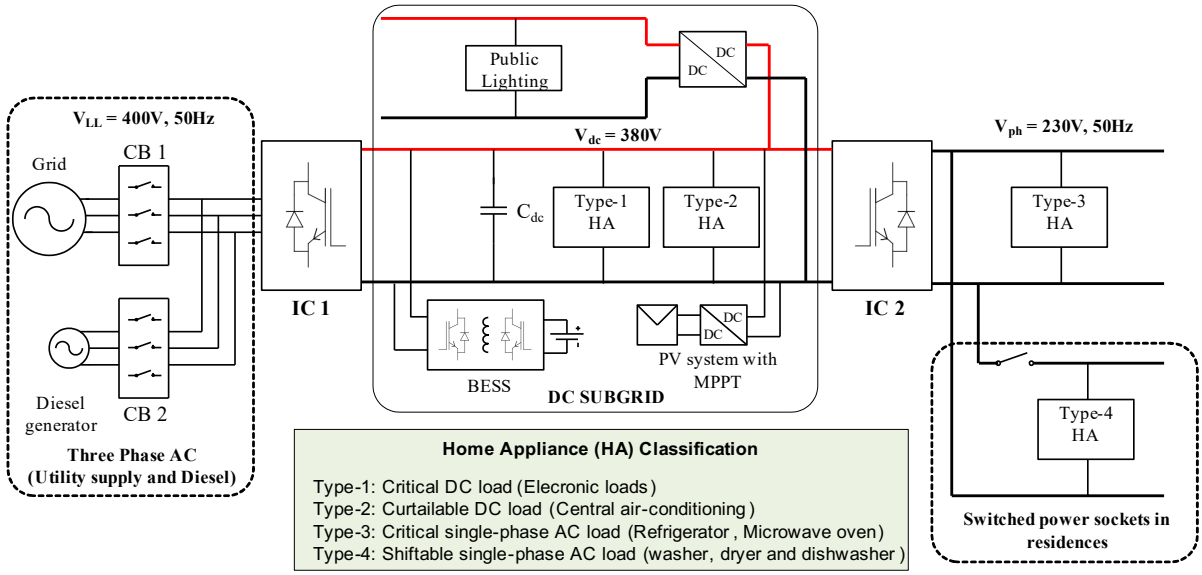


**Fig. 3. Demand Response implementation in the transitional microgrid.**

This design of building energy management system addresses the four main community challenges in increasing the residential demand flexibility: (1) today's home energy management system (HEMS) industry provides vendor-specific systems that are controlled by proprietary software and are not compatible with home-automation devices sold by other vendors, thereby creating a "walled garden". This may lead to the consumer being stuck with a failed platform; (2) the cost of commercial HEMS products is high, and their benefits are not understood by the public; (3) as more energy efficient DC-fed loads are developed, existing distribution systems may not support them; and (4) perceived threats to security and privacy. These reasons lead to only a small percentage of residents actually adopting an HEMS. Therefore, a large section of the flexible demand is left untapped. We tackle these concerns by proposing a shift from the policy of voluntary HEMS installation (see Fig. 4), to providing in-built, controllable smart sockets within all the residences in the building. These would be controlled at the building level, which is modelled on the transitional microgrid topology. This infrastructure can be used as a hardware platform by any competent third-party using their own software to interact with the market and control the Building Energy Management System (BEMS) of the residential building.

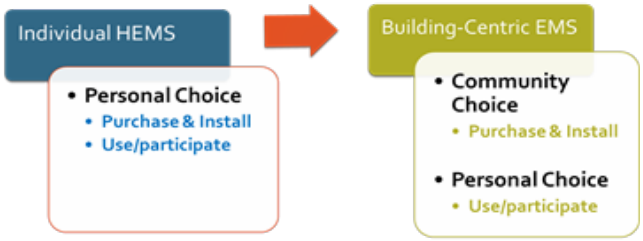


**Fig. 4. HEMS vs. BEMS.**

The HA in each residence are classified into four categories, or 'Types', as shown in in Fig. 3 (inset). Type-1 and Type-2 loads are directly connected to the DC bus. Type-3 loads are connected to the output of IC2, while Type-4 loads each have an electronically controlled relay that controls their power supply. The relays in all homes are controlled by the central BEMS. This is a simple alternative to installing vendor-specific HEMS in every home. With this hardware configuration, all the residents are enrolled into the DR scheme by default and given an option to opt out if they require (libertarian paternalism). Note the timeline of installation of the proposed BEMS and hardware shown in Fig. 5 and compared to the status quo. For our design, this investment would be done right after the construction of the residences, within the "window of opportunity" according to the habit discontinuity effect. Further, this cost is shared by all the residents, and is therefore more attractive to individual residents. The resultant profit for the community is also higher because the total flexible demand is larger, and better contracts for DR can be negotiated with the utility. Fig. 5 also illustrates the difficulty in achieving 100% penetration among all residents using only voluntary HEMS installations.

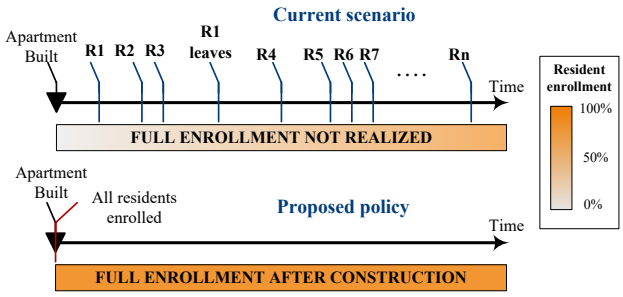


**Fig. 5. Timelines of the current and proposed policies showing resident enrollment into a DR program. The status quo is characterized by residents R1, R2, …, Rn voluntarily installing HEMS and dropping out at arbitrary times, while full enrollment is ensured in the proposed framework.**

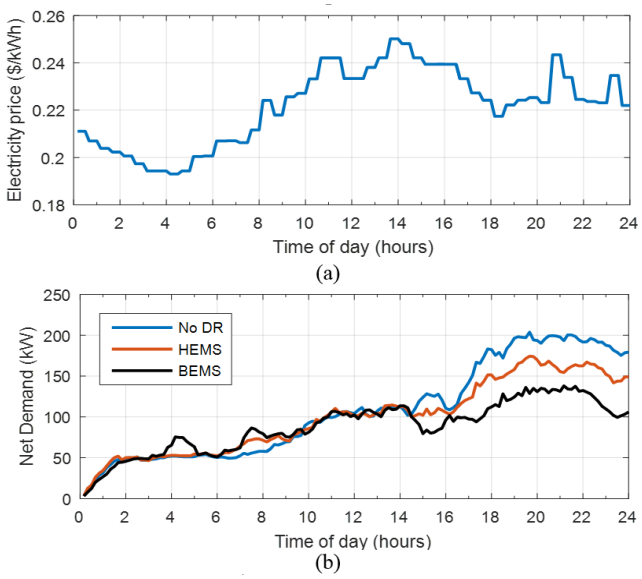


**Fig. 6. (a) Day-ahead electricity price, and (b) comparison of the load profiles for scenarios 1-3.**

Note that this simple on/off DR scheme is only a representative implementation, and any complex smart device can replace the switches shown in Fig. 3. In such cases, interoperability can be ensured by using a common DR standard such as OpenADR.

The proposed BEMS strategy is implemented for a typical apartment building in Singapore as a case study: a 16-floor building, with 96 residences in it. For a realistic setting, we assume that the building is divided equally into residences of two different sizes: four-room homes, and five-room homes. To simulate the DR scheduling process, we use the day-ahead electricity price data obtained from the Singaporean Energy Market Company, which is shown in Fig. 6(a). We consider the following scenarios for comparison:

- *Scenario 1:* No DR program implemented.
- *Scenario 2:* Voluntary HEMS installation. The demographic composition of the building occupants is obtained from Singaporean census data. We assume that of all residents, only half of the young families can afford, and are willing to install HEMS systems. We further apply typical times of use of HA for the different types of households as constraints in the simulation.
- *Scenario 3:* Proposed BEMS system. All residents participate in the DR program. We consider typical times of use of HA as constraints in the simulation.

The net load profiles for the apartment generated for the above scenarios are shown in Fig. 6(b). The energy cost per day, and the peak power demand for the entire building are presented in Table III. Clearly, the benefits in terms of the reduction of the daily electricity cost, and the peak demand is higher for the proposed BEMS system than when some residents voluntarily installing HEMS in their homes. While this is as expected, the main takeaway is not the magnitude of this difference, but that all residents are now involved in the DR program, or can be involved if they wish to. Note that the magnitude of cost savings would be higher if the price were demand-sensitive. Further, in the proposed BEMS approach, it is possible to use community resources such as battery generation, diesel generation, or photovoltaic generation to optimize energy consumption as well, which is not possible in individual HEMS installations.

**Table 1. Simulation Results with Demand Response Implementation.**

| | Cost ($/day) | Peak demand (kW) | Reduction in cost (%) | Reduction in peak load (%) |
|---|---|---|---|---|
| No DR | 591.52 | 203.76 | - | - |
| HEMS | 541.75 | 174.31 | 8.40 | 14.45 |
| BEMS | 479.01 | 138.03 | 19.02 | 32.23 |

**Multi-microgrid stability analysis**

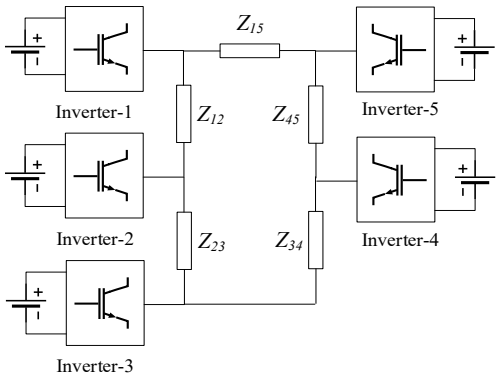


The transitional topology detailed previously consists of an inverter that interfaces each microgrid to the power grid, at the point of common coupling. This body of work focuses on the impact on the distribution system when multiple such residential microgrids are in operation (see Fig. 7). For this, we consider that the droop control is employed to share power amongst the different microgrids. For the current period of the project, the focus has been on modeling the stability behavior of such multi-microgrid systems, with a view to analyze and address the various instability factors involved.

The model of the multi-microgrid was developed with the following assumptions:

1. The inner-loops of the inverters- viz., the voltage and current PI loops do not affect the low-frequency modes of the system.
2. The distribution system dynamics are modeled by the first-order Taylor's series approximation of the real and reactive power flow equations.

The first assumption does not lead to any significant errors in the model, as is well known from existing literature. The second assumption entails the use of a more-detailed model that incorporates the distribution system dynamics, as opposed to conventionally used static models; this is therefore beneficial to the purposes of our study. Pursuant to these assumptions, the main modeling equations can be written as follows:

$$f = f_0 - k_f \left[\frac{\omega_c}{s+\omega_c}\right](P - P_0) \tag{3}$$

$$V = V_0 - k_v \left[\frac{\omega_c}{s+\omega_c}\right](Q - Q_0) \tag{4}$$

$$\begin{bmatrix}\Delta P\\ \Delta Q\end{bmatrix} = -\begin{bmatrix}B(s) & -G(s)\\ G(s) & B(s)\end{bmatrix}\begin{bmatrix}\Delta\delta\\ \Delta V\end{bmatrix} \tag{5}$$

Here, P and Q refer to the real and reactive power output of each inverter, f and V, the output frequency and voltage, $\omega_c$, the power filter cut-off frequency and δ, the phase angle of the voltage. The dynamic Jacobian elements G(s) and B(s) can be obtained from the first-order Taylor's series expansion of the Jacobian elements. From the equations (3)-(5), the eigenvalues of the multi-microgrid system can be obtained, and their damping, calculated.

**Identifying destabilizing effects**

The destabilizing effects in multi-microgrid systems with droop control can be broadly classified into two types (1) real and reactive power cross-coupling and (b) distribution system dynamics. The first phenomena, cross-coupling has been already studied extensively in literature, and is therefore not covered here. However, the second- the distribution system dynamics, has not been studied separately. For this, we propose a novel approach using generalized droop, which eliminates the cross-coupling. The proposed control schematic is shown in Fig. 8. In such a case, all the remaining instability effects arise purely from the distribution system dynamics.

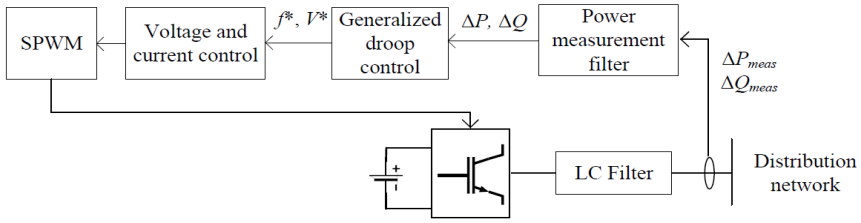


**Fig. 8. Control schematic of an inverter with generalized droop.**

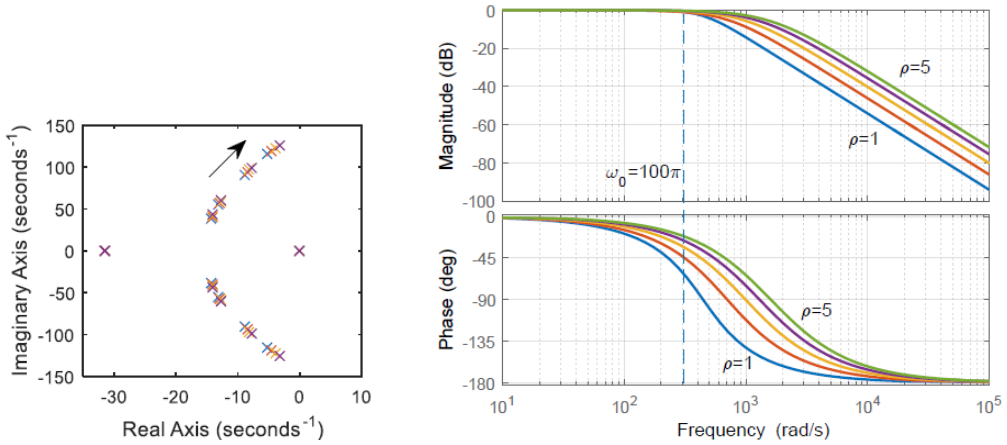


**Fig. 9. *Left*- Plot of eigenvalues as the droop gains are increased, indicating impending instability at higher values of droop. *Right*- Bode plot of 1/DSLF for various R/X ratios indicating significant phase lag at power frequency, which is the primary cause of instability due to distribution system dynamics.**

Analyzing the small-signal with the generalized droop, the following important conclusions can be obtained:

1. The instability due to the distribution system dynamics can be attributed to three effects- (1) Distribution System Lag Factor (DSLF), (2) EM-induced cross-coupling and (3) EM-induced damping.
2. The DSLF is the main factor that leads to destabilization. The other two effects are not concerning as long as the effect of the DSLF is annulled.
3. The destabilizing effects of the DSLF are more significant for lower values of R/X ratios, as the lag for higher R/X ratios becomes negligible.
4. The effect of the DSLF can be canceled with appropriate redesign of the power measurement filter. This requires no additional hardware modification or sophisticated computing power.

The above observations can be verified from Fig. 9. Pursuant to these findings, the compensator design can be carried out in a systematic manner, in contrast to previous works in literature, which relied on the trial-and-error principle.

**Mitigating the effects of distribution system dynamics**

We developed a high-level linear model of the multi-inverter system in terms of the droop gains, the droop rotation matrix, and the network admittance and susceptance, as follows:

$$\begin{bmatrix}\boldsymbol{\Delta f}\\ \boldsymbol{\Delta V}\end{bmatrix} = -\frac{1}{T_c s+1}\boldsymbol{T}\begin{bmatrix}\boldsymbol{K_f} & \boldsymbol{0}\\ \boldsymbol{0} & \boldsymbol{K_v}\end{bmatrix}\begin{bmatrix}\boldsymbol{\Delta P}\\ \boldsymbol{\Delta Q}\end{bmatrix} \tag{6}$$

$$\boldsymbol{\Delta f} = \frac{1}{2\pi} s\,\boldsymbol{\Delta\delta} \tag{7}$$

$$\begin{bmatrix}\boldsymbol{\Delta P}\\ \boldsymbol{\Delta Q}\end{bmatrix} = -\begin{bmatrix}\boldsymbol{B}(s) & -\boldsymbol{G}(s)\\ \boldsymbol{G}(s) & \boldsymbol{B}(s)\end{bmatrix}\begin{bmatrix}\boldsymbol{\Delta\delta}\\ \boldsymbol{\Delta V}\end{bmatrix} \tag{8}$$

Combining the above models, the combined system model can be obtained as:

$$\left(\frac{\left(\rho+\frac{s}{\omega_0}\right)^2+1}{\rho^2+1}\begin{bmatrix}s(T_c s+1)\boldsymbol{K_f^{-1}} & \boldsymbol{0}\\ \boldsymbol{0} & (T_c s+1)\boldsymbol{K_v^{-1}}\end{bmatrix} - \begin{bmatrix}\widehat{\boldsymbol{B}} & \boldsymbol{0}\\ \boldsymbol{0} & \widehat{\boldsymbol{B}}\end{bmatrix} + \frac{s}{\omega_0}\begin{bmatrix}-\boldsymbol{B}\sin\phi & -\boldsymbol{B}\cos\phi\\ \boldsymbol{B}\cos\phi & -\boldsymbol{B}\sin\phi\end{bmatrix}\right)\begin{bmatrix}\boldsymbol{\Delta\delta}\\ \boldsymbol{\Delta V}\end{bmatrix} = \boldsymbol{0} \tag{9}$$

From the above model, it can be observed that the instability arises due to the Distribution System Lag Factor (DSLF), which is the coefficient of the first matrix in the above characteristic equation. The other effects due to line dynamics, viz. EM-induced cross-coupling and damping have a small impact on the eigenvalues and can be theoretically demonstrated to not cause instability. Since the DSLF is the sole destabilizing factor, it is intuitively obvious that it needs to be canceled through appropriate control, i.e., a lead-lag compensator. From the model (9), it is easy to see that the phase lead provided by the compensator should be exactly equal to the phase lag of the DSLF. This directly yields the analytic design of the compensator as:

$$F(s) = \frac{\frac{s^2}{\omega_0^2}+2\frac{\rho s}{\omega_0}+1+\rho^2}{(1+\rho^2)(T_c s+1)(\tau s+1)} \tag{10}$$

In contrast to prior works, we no longer need to depend on empirical tuning procedures to obtain the compensator. Moreover, previous works are not consistent in terms of the order of the filter required, or whether the modifications are to be done in both the frequency and voltage loops. In contrast, based on the analysis done in our work, the required order of the filter is definitively identified as 2. Further, we see that the compensation needs to be done for both the voltage and frequency loops, as the Distribution System Lag Factor (DSLF) appears in the voltage-dynamics-characteristic-equation as well.

On implementing the proposed filter, the pole plots in Fig. 10 show that a previously unstable system now becomes stable, due to the cancellation of the poles corresponding to the distribution system dynamics. Moreover, due to the EM-induced damping effect, the new pole pairs are curved left-ward with the proposed filter, in contrast to before.

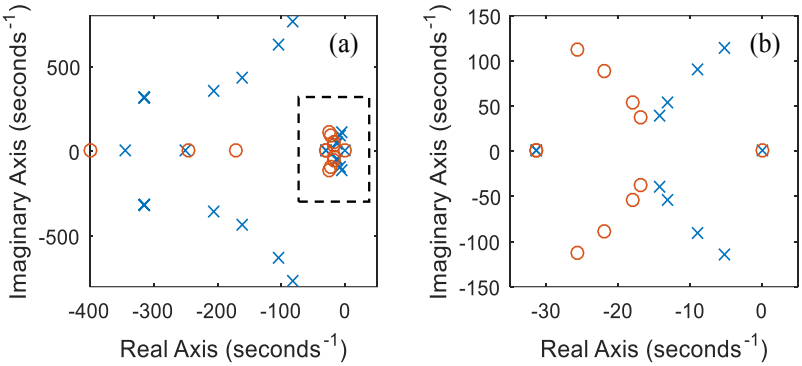


**Fig. 10. Juxtaposition of the system poles under generalized droop for the same droop gains with the conventional filter (blue x) and proposed filter (red o), indicating recovery of stability under the proposed filter.**

The proposed filter design is generic and applicable to different types of droop control, including conventional droop, which is the most common. This is demonstrated in Fig. 11, where it can be seen that the stability region significantly expands under low R/X ratios. In fact, in such cases, the stability region becomes nearly infinite, as the P-Q cross-coupling effect is also low for low R/X. This also serves to prove that the effect of the P-Q cross-coupling and the distribution system dynamics can be separately viewed and addressed, independent of each other.

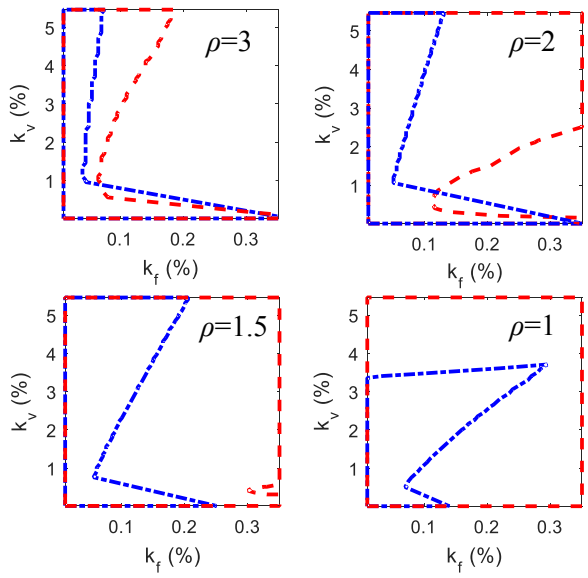


**Fig. 11. Stability region comparison for the conventional P-f/Q-V droop control with the conventional filter (blue dash-dot) and proposed filter (red dashes) for different values of R/X ratios ($\rho$). The stability region significantly expands under low R/X ratios, where the DSLF is the most dominant.**

**<u>Optimal damping recovery scheme</u>**

In multi-inverter systems, despite the best efforts to design a droop control scheme for guaranteeing the stability, instability can still occur due to the following reasons:

- Partial implementation of the proposed (advanced) droop control schemes
- Contractual restrictions to implementation of advanced schemes, or hardware limitations in legacy systems
- Presence of synchronous generators (e.g., diesel generators) whose droop characteristics cannot be changed
- Unexpected change in the network topology.

Therefore, there is a need to design mechanisms to recover the stability in real-time when instabilities occur. The following are the main challenges to developing such a scheme:

- There is a need for centralized implementation of damping recovery, since stability is a global phenomenon that depends on the parameters of all the inverter and the network parameters. This leads to the problem of scalability.
- Recovery of stability entails changing the droop gains, which leads to disproportionate power sharing amongst the various inverters.

To address the above challenges, we proposed a sensitivity-based damping recovery scheme, implemented as shown in Fig. 12. Here, the droop gains of the inverters are reduced in decreasing order of sensitivity, whereby the damping recovery occurs in the fastest possible time, and with the minimum possible disruption to the power sharing proportion. The advantage of such a scheme is that it is also applicable to systems with synchronous machines whose droop gains are not adjustable. Further, the use of an event-triggered framework as shown reduces the communication rate under normal operation.

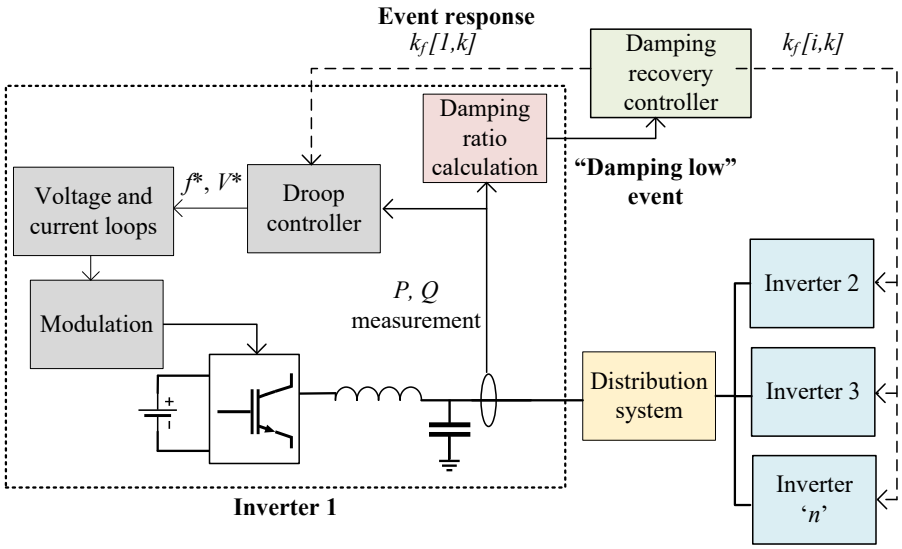


**Fig. 12. Control schematic for implementing the proposed damping recovery scheme.**

The main features of the proposed damping recovery scheme are as follows:

- The interconnecting impedance is used as a measure of the criticality of each inverter, which enables the calculation of the sensitivity in a decentralized manner. This reduces the computational complexity from $O(n^3)$ to $O(n)$.
- The proposed method minimizes the compensation effort and time
- The power sharing proportions are largely preserved after damping recovery.

Some of these advantages can be quantified in the results from Fig. 13. The proposed method has the smallest power sharing disparity. In comparison, while single-point correction achieves the damping recovery in the fastest time, the power sharing disparity is extremely high. Moreover, the proposed method is also robust to communication loss, as the sensitivity-based scheme yields the most optimum scheme even under communication failure. While the damping recovery time can slightly increase, the required damping ratio is nevertheless ultimately obtained.

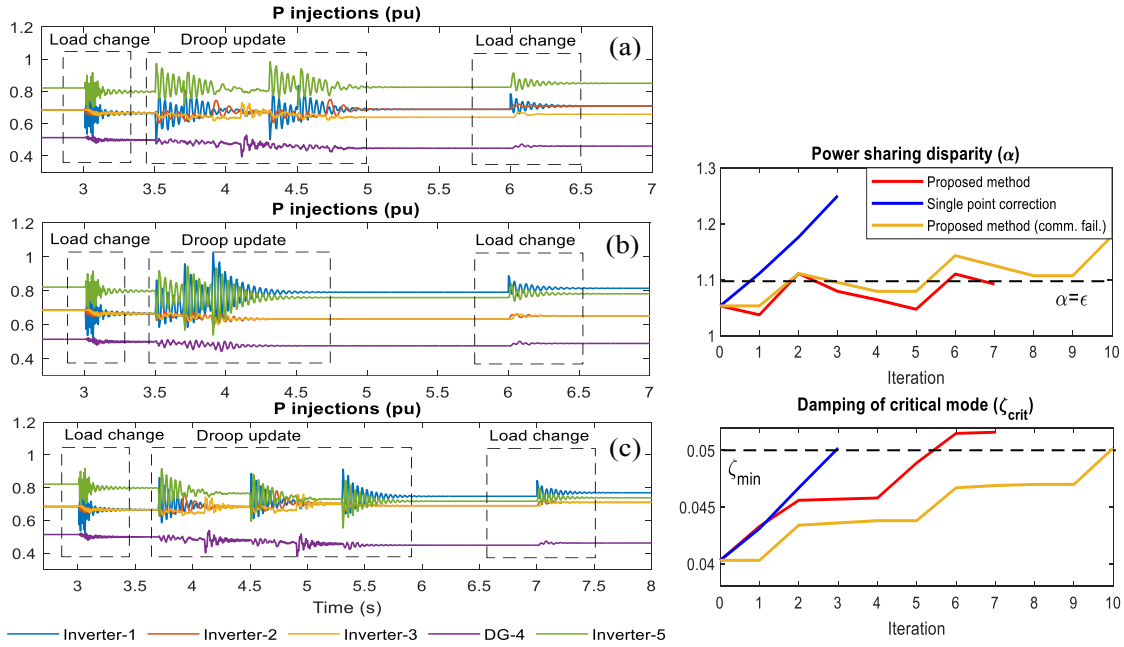


**Fig. 13. Left- Power outputs obtained from the IEEE 123 bus test system for (a) the proposed method (b) single-point correction and (c) communication failure at the most sensitive node. Right- Plots of power sharing disparity and system damping for the same case studies.**

**Stabilization of the inverter-based system based on critical clusters**

In addition to the above analysis, there is a remarkable case when the active and reactive power droop coefficients ratio is uniform across the system, i.e. in matrix terms $\boldsymbol{K_f} = k\boldsymbol{K_v}$. With this representation, the poles λ of the dynamic model (4) are connected with the eigenvalues $\mu_i$ of the weighted network susceptance matrix $\boldsymbol{C} = \boldsymbol{K_f B}$ as follows:

$$\mathrm{T_c} k f(\lambda) + g(\lambda)(k + \mathrm{T_c}\lambda)\mu_i + \mu_i^2 = 0 \tag{11}$$

Where $f(\lambda) = \lambda g^2(\lambda)[h^2(\lambda) + 1], g(\lambda) = (1 + T_c\lambda), h(\lambda) = \left(\rho + \frac{\lambda}{\omega_0}\right).$

Thereby, the stability analysis of the whole system (4) reduces to the analysis of polynomials (11) for all values of $\mu_i$. Each polynomial in (6) (i.e. polynomial with a specific $\mu_i$), in fact, corresponds to five distinct modes of the initial system and can be thought of as a representation of an equivalent two-bus system - a *cluster*. Thus, the initial microgrid can be effectively split into separate clusters utilizing the spectrum of the weighted network susceptance matrix $\boldsymbol{C} = \boldsymbol{K_f B}$. Fig. 14 shows an example of such a split for the two-area system with four inverters. Dominant low-frequency modes are presented in the pole-zero plot of Fig. 15, where each pole pair corresponds to the individual cluster in Fig. 14.

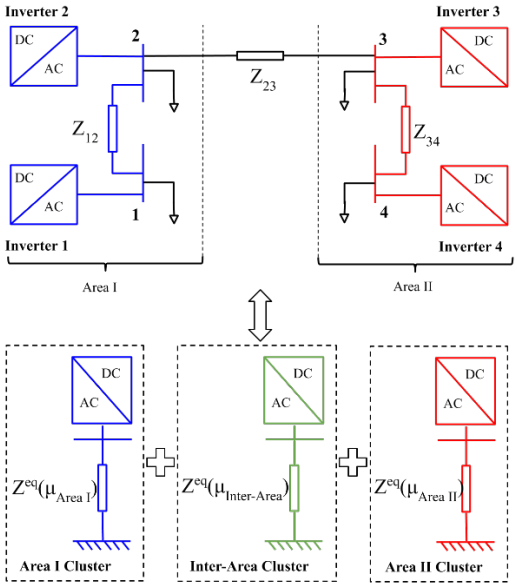


**Fig. 14. The proposed decomposition - the larger two-area system splits into a set of clusters, equivalent two-bus systems.**

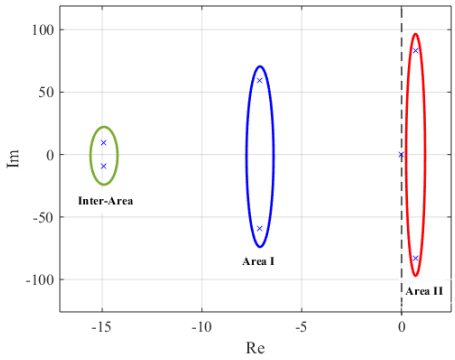


**Fig. 15. Dominant modes for the two-area system of Fig.14, showing the local modes in Area I and Area II as well as the inter-area mode between both areas.**

It is important to note that all the roots of equation (11) have a negative real part if the corresponding $\mu_i$ is less than a certain value $\mu_{cr}$. If all $\mu_i < \mu_{cr}$, then the system is stable, and vice versa; if there some $\mu_i > \mu_{cr}$, $i = 1, \cdots, u$, then the system has $u$ unstable modes. Hence, $\mu_i$ are the key values for stability assessment of the system, so that parameters of the system that affect the corresponding $\mu_i$ most are also the ones that should be changed to gain stability margin. We found out that these parameters to be changed are associated with high values in the corresponding eigenvector $\boldsymbol{\psi_i}$ using the sensitivity analysis. Therefore, the proposed procedure depicted in Fig. 16 is based on the values of $\mu_i$ and $\boldsymbol{\psi_i}$.

The proposed methodology was verified numerically using the two-area system with four inverters. Following the procedure for critical cluster identification in Fig. 16, we find that $\mu_{cr} = 1.97$ for the chosen values of $\rho = 1.4$ and $k = 3$. Next, eigenvalues of the weighted Laplacian matrix $\boldsymbol{C}$ were calculated as $\mu_1 = 0$, $\mu_2 = 0.93$, $\mu_3 = 1.05$, and $\mu_4 = 2.06$. According to our results, the system was unstable because $\mu_4 > \mu_{cr}$. Further, by exploring the corresponding eigenvector $\boldsymbol{\psi}_4 = [-0.02, 0.06, -0.73, 0.69]^{\mathrm{T}}$, we concluded that inverters 3 and 4, and line 3-4 brought the most contribution to the unstable cluster. Further, we varied different system parameters and directly verified the corresponding changes in eigenvalues $\mu$, with simultaneous direct dynamic modeling of the system to show its stability/instability. For example, the stabilization of the system by changing the length of the line 3-4 is demonstrated in Fig. 17.

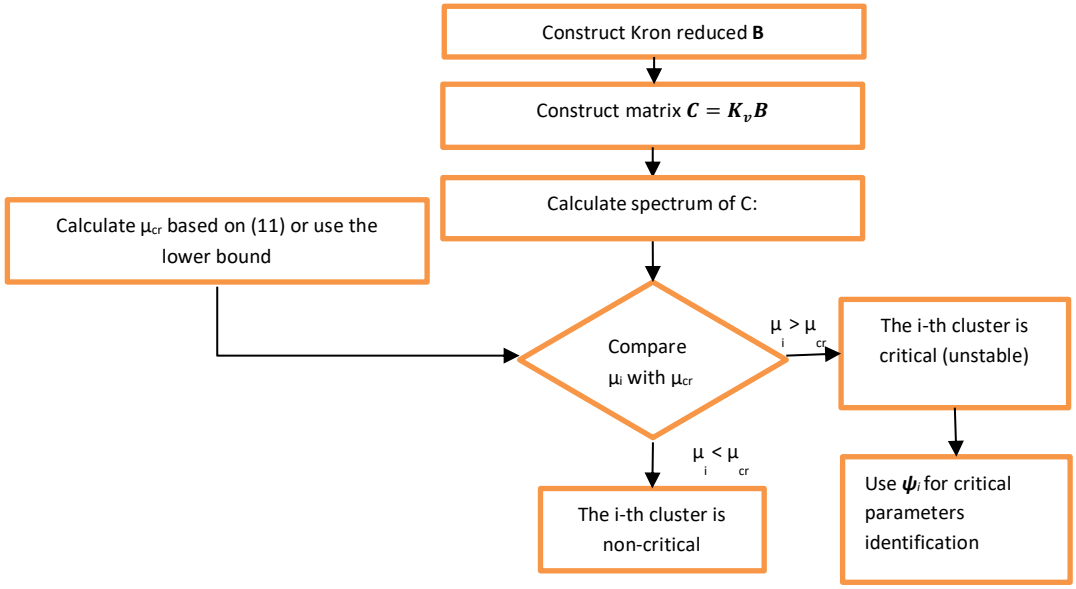


**Fig. 16. Flowchart to identify the critical clusters and parameters.**

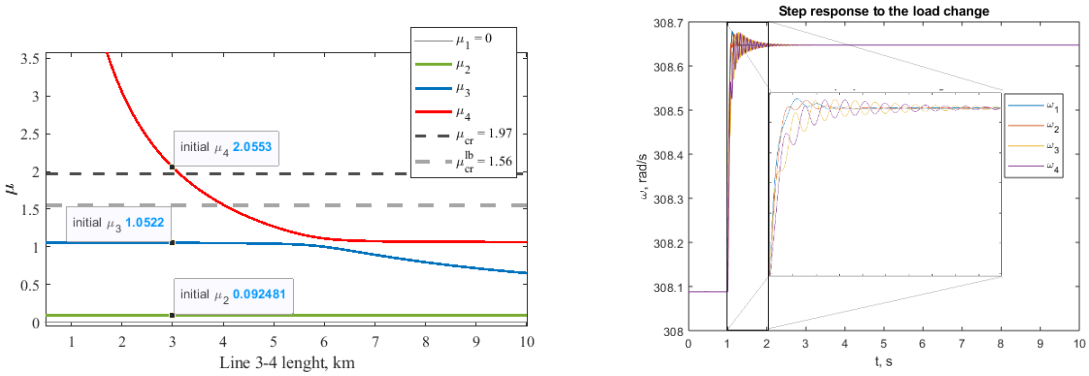


**Fig. 17. Spectrum $\mu_i$ versus the length of line 3-4, $l_{34}$, in Area II (the left plot) and the step response subjected to a 10% load change with increased $l_{34} = 4\ km$ (the right plot). The increase in the line length stabilizes the system.**

Thereby, we showed that for critical clusters, stability is primarily affected by the length of lines (or impedance) and droop gains. The former provides useful insights for grid planning studies, while the latter benefits system operation. We explicitly demonstrated that to stabilize an inverter-based system, one should mostly target parameters of the critical clusters - droop coefficients of the corresponding inverters and/or lines connecting them. We also showed that tuning inverters associated with non-critical clusters are futile in regaining network stability. Thus, this project established the technical principles to explain the oscillatory interactions among inverters and designed an effective procedure to enhance/restore system stability most efficiently.

**<u>EV charging optimization based on day-ahead pricing</u>**

We consider historical data consisting of a set of consumers' residential demands, and their corresponding EV charging schedules. This data is split into weekdays and weekends, as typically, living habit on weekdays and the weekends for most households are very different.

The 'ideal' demand curve with the minimum possible peak demand is determined while keeping the total power demand constant (see Fig. 18 and 19). This desired total demand curve is based on the total electricity demand of all the households over one year, for the purpose of minimizing the peak demand and smoothing the curve. This means that the EV charging power would be preferably allocated to the timeslots with a smaller residential demand.

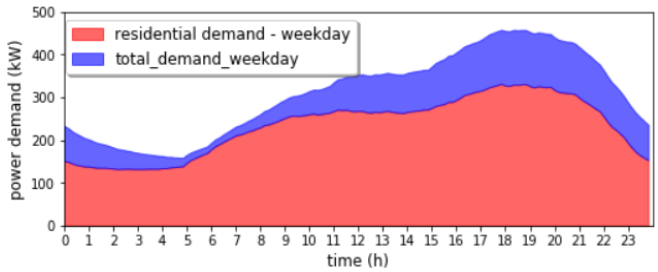


**Fig. 18. Original residential-only and total demands of the community.**

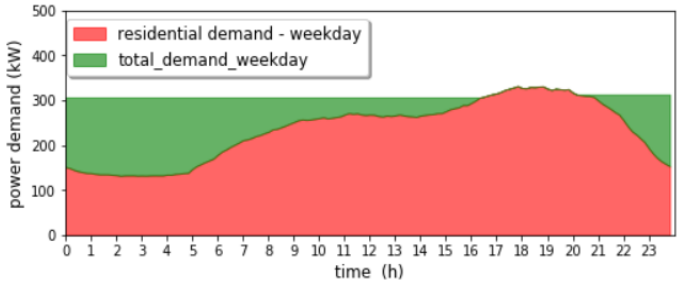


**Fig. 19. The 'ideal' power demand of the community.**

A day-ahead pricing model is presented to achieve the ideal consumption profile. The concession of comfort preference for consumers to charge EVs is attractive because charging is used to store energy in advance instead of real-time use as other appliances. EV charging can be turned on or off with intelligent-based control of smart meters without violating the minimum off-on interval. Therefore, the price is an incentive strategy for consumers to modify their charging time, while maintaining a balance between the cost and convenience. We would like to determine how much concession a consumer would make when the price is for the curve nearest to the ideal profile.

We define a parameter called Comfort Tolerance, which measures how much concession customers would give to comfort in order to achieve the least electricity cost that would result in the ideal demand curve. A higher value of tolerance reflects that the customer would compromise more comfort in exchange for monetary benefit. Once the total number of available charging timeslots is determined, EV users are selected randomly in the order of descending charging probability for each household. This means that timeslot allocations are not fixed; there is an inherent randomness in the allocation process. For this, a roulette wheel selection scheme is proposed. Finally, we develop an optimization model whose objective is to determine the optimal charging time and power such that the electricity cost is minimal, while at the same time being constrained in terms of the charging level, storage capacity, and consumers' convenience.

In order to evaluate the proposed EV scheduling model, we refer to the 2009 RECS data set for the Midwest region of the US. This includes the historical demand profiles for 200 households, as well as in-home EV-charging behaviors for 256 EVs present in these households, assuming Level 1 (1.92 kW) residential charging infrastructure. Realistic load profiles are simulated, which reproduce realistic residential power consumption patterns and EV charging profiles. We assume that all of these households belong to a single community, and the data represent the net system demand. A day is divided into 144 timeslots, each with a duration of 10 minutes, starting at 12:00AM (midnight). The average electricity usage for residential and (residential + EV charging) profiles from this dataset is depicted in Fig.18. From the data above, the ideal electricity demand curve is designed, and shown in Fig. 19. From this figure, we see that the peak demand of the residential curve is high during weekdays. If the EV charging were to happen completely at periods away from the peak period (the desired EV charging behavior of the community), the peak demand of the total system would now equal the peak residential demand. From the difference of the ideal and original curves, the day-ahead price curve is obtained. Finally, to make the price curve reasonable and close to practical values, lower and upper

bounds are set to be 15 ¢ / *kWh* and 20 ¢ / *kWh*. As shown in Fig. 20, the lower price corresponds to a bigger difference of the two curves with the aim to encourage customers charging more during this period. Thus, EV-charging optimization is introduced based on this price profile, the results of which are explained in the sequel.

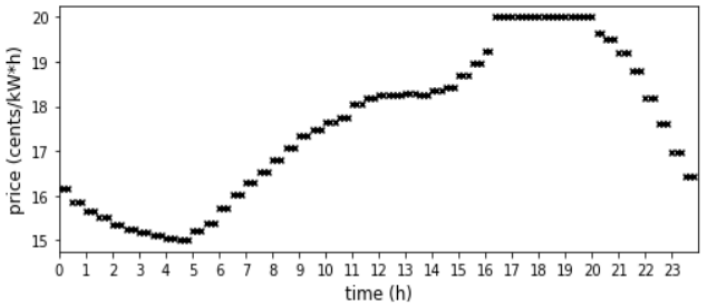


**Fig. 20. The desired day-ahead price curve.**

For a test community comprising of 200 households, day-ahead EV scheduling is adopted with the assumption that all households are enrolled into the scheme. As mentioned previously, the available charging time are chosen randomly based on their charging probability. To account for the randomness, each EV optimization is processed for 20 times. The boxplots for the total residential and EV-charging demands after optimization are obtained and presented in Fig. 21.

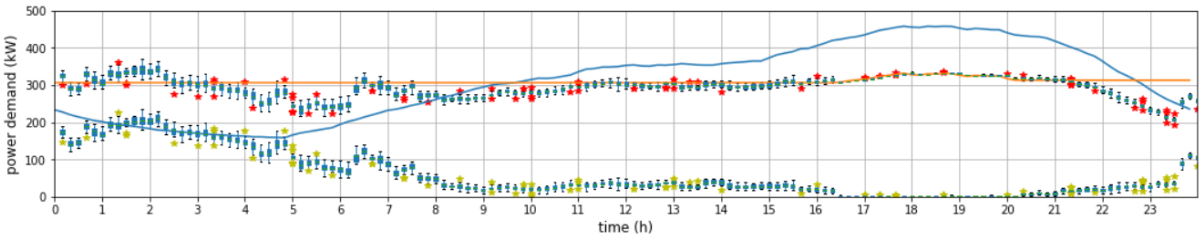


**Fig. 21. Residential demand after optimization. The blue and orange curves respectively denote the total system demand before optimization, and the ideal (desired) system demand. The box plots with the green and red outliers respectively denote the EV and total system demands after the proposed optimization process.**

This figure shows that the system demand is close to the ideal profile, with a significant reduction in the aggregate peak demand. Again, this result is for 200 households; when the size of the community increases, peak demand for the whole community can be reduced to a larger extent, as more and more EVs are available for optimization. The corresponding ramp rate is presented in Fig. 22, with shows that ascent or descent rate is within an acceptable range of [-4kW/min, 5kW/min], about 1% of the total demand.

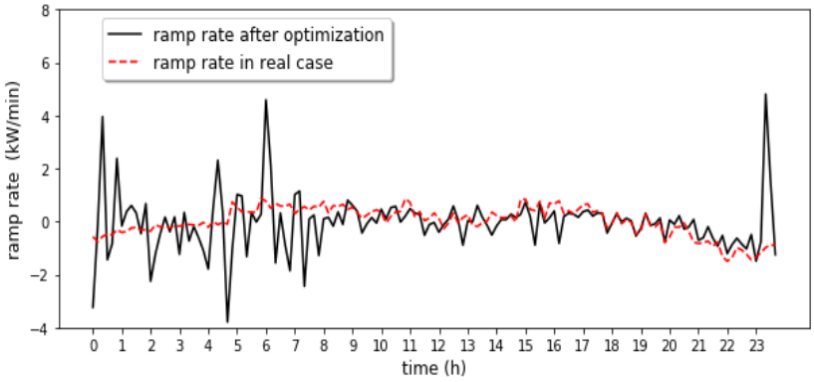


**Fig. 22. Ramp rate of the total electricity demand after optimization.**

**Effective residential demand response design**

Incentive-based DR programs require changes in the consumers' demand patterns--usually, a load reduction during a specified event period--in exchange for monetary rewards. Event details, including the event timing and incentive, are communicated to the DR participants before the actual event period. However, real-time feedback about their performance during the event may not available to the consumers. Any data collected about the consumer performance is only used for post-event analyses, primarily for billing purposes (see Fig. 23(a)). In this open loop implementation, the expected quantum of peak energy savings may not materialize due to multiple factors. While studies have shown the importance of real-time consumer feedback in eliciting short- and long-term behavioral change in consumers, such feedback mechanisms have not been incorporated by grid operators.

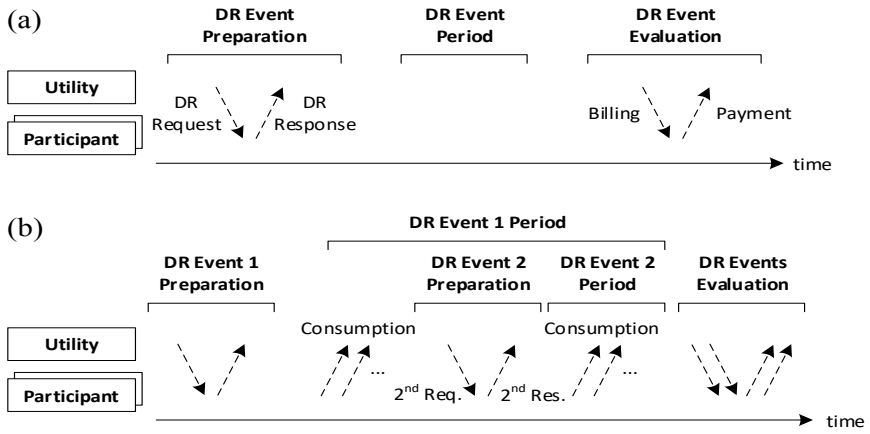


**Fig. 23. Incentive-based DR program design: (a) traditional approach, and (b) proposed multi-event design.**

To address these challenges, our research proposes monitoring of the DR performance in real-time to predict potential non-compliance of the system to the DR goals during the DR event. In conjunction, the proposed scheme increases the incentive offered to the participants to annul any deficit in the response. Different to existing studies, the higher incentive is implemented using a second DR event, rather than the more impractical alternative of continuously varying the incentive in a closed loop. The second DR event happens within the time frame of the first DR event, as illustrated in Fig. 23(b).

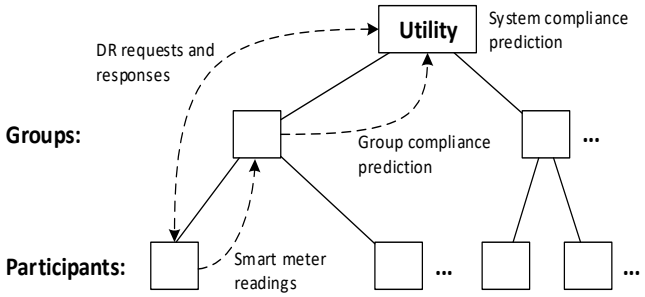


The proposed monitoring system is schematically depicted in Fig. 23. The system compliance to the DR goals can be predicted by assessing the performance of the consumers at either the individual consumer level, or by grouping them as shown. This allows the estimation of compliance to be more accurate by eliminating to an extent the uncertainty and unpredictability of individual residential consumers in the community. Moreover, a group-based design would allow distributed data processing and communication, which would significantly reduce the computation and communication overheads. This also lends scalability to the design.

Once the system operator predicts that the response at the end of the DR event would be unsatisfactory, it may then offer higher incentives for consumers to offset the deficit in the energy reduction. Here, rather than dynamically changing the incentive for all the consumers, we propose the incentive change to be implemented as a *second* DR event (see Fig. 23(b)). This way, by preserving the schema of the DR event, the proposed design allows for easier implementation by the operator. The only changes necessary for the second DR event would be the event timing and incentive. While the second event is

announced at short notice, participants only need to reconsider their energy usage in the immediate future, and therefore does not involve much preparation. Note that we do not consider more than two DR events to avoid the risk of participation fatigue.

The proposed monitoring process is adaptively changed as the DR event progresses. In particular, adaptiveness is achieved by reducing the monitoring rate at the various levels of the infrastructure once the compliance assessment is complete. Say a group of DR participants is predicted to be non-compliant at some point during the DR event. For this group, further compliance testing is not performed during the DR period. Hence, the monitoring rates for smart meters in this group can be lowered to the rate required for billing purposes. Meanwhile, the monitoring in the other groups remains unaffected, and the system-level monitoring query continues to predict the system-compliance status. Once the overall system is detected to be non-compliant, the monitoring rate for all the smart meters is reduced.

Using a simple compliance assessment technique based on the comparison of the participants' expected and actual demand profiles during the DR event, and the average load profiles depicted in Fig. 24, simulations were carried out for a system of 100,000 residential consumers. We also assume that 22.5% of the residents own an electric vehicle.

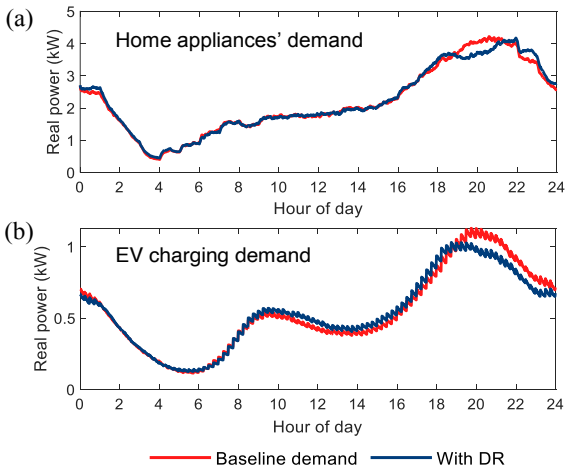


**Fig. 24. Average load profiles (in kW) for (a) home appliances in one residence, and (b) charging one residential EV.**

Sample load profiles resulting from our simulations are depicted in Fig. 25. Clearly, incorporating feedback and subsequently varying the incentive offered to the participants increases the overall demand response and the peak demand reduction.

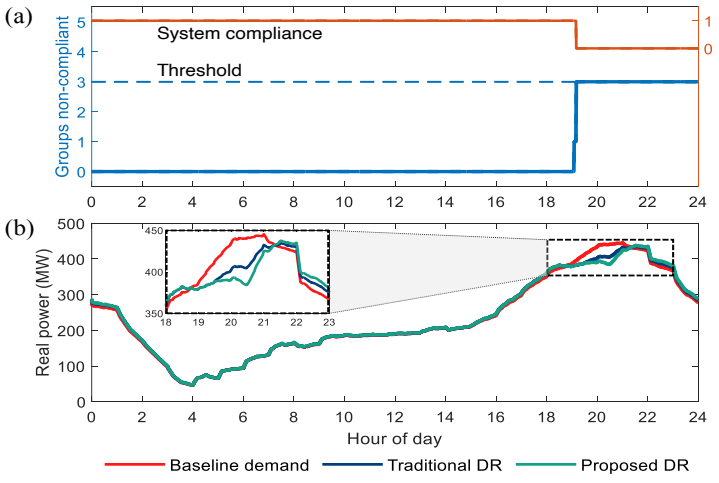


**Fig. 25. Illustrating the proposed DR scheme for a DR event from 6:30pm to 8:30pm.**

The impact of the second DR event is conditioned upon the new incentive offered, and Fig. 26 illustrates this effect. This heat map could be used by the operator while deciding the incentive that needs to be offered during the second DR event. In general, we find that higher the incentive, the better is the response.

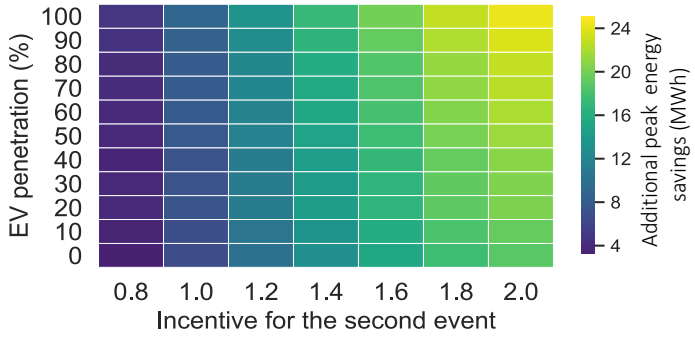


**Fig. 26. Additional peak energy savings (in MWh) in the proposed DR design over the traditional single-event design.**

## 4. References to the Research

### a) Publications

The findings from this project were published in top-tier peer-reviewed journals:

1. J. Zhang, S. Sahoo, J. C. -H. Peng, and F. Blaabjerg, "Mitigating Concurrent False Data Injection Attacks in Cooperative DC Microgrids," IEEE Transactions on Power Electronics, Early Access.
2. J. Soon, G. Raman, J. C. -H. Peng, and D. D. C. Lu, "Current Ripple Reduction Using AC Core Biasing in DC-DC Converters," IEEE Transactions on Industrial Electronics, Early Access.
3. J. Soon, D. D. C. Lu, J. C. -H. Peng, and W. Xiao, "Reconfigurable Non-Isolated DC-DC Converter with Fault-Tolerant Capability," IEEE Transactions on Power Electronics, vol.35, no.9, pp. 8934-8943, 2020.
4. G. Raman, J. C. -H. Peng, and H. Zeineldin, "Optimal Damping Recovery Scheme for Droop-controlled Inverter-based Microgrids," IEEE Transactions on Smart Grid, vol.11, no. 4, pp. 2805-2815, 2020.
5. G. Raman, and J. C. -H. Peng, "Mitigating Stability Issues due to Line Dynamics in Droop-Controlled multi-Inverter Systems," IEEE Transactions on Power Systems, vol. 35, no. 3, pp. 2082-2092, 2020.

### b) Breakthroughs

This research proposed a new stability theory in managing inverter-based renewable generations within a microgrid. Different from prior studies, this project showed that there is a previously-unknown source of instability in microgrids, one that pertains to the dynamics introduced by the electromagnetic behaviour of the power lines in the grid. The project also provides simple and effective control solutions to guaranteeing network stability under most operating conditions. These outcomes are critical breakthroughs for establishing a more power electronic grid of the future.

### c) Other Notable Achievements

We developed a hands-on design project for educating students and engineers on microgrid stability and inverter operation. The project tasks translate the research findings of this Tier-1 project into a step-by-step process that can be applicable to any system. An educational hardware microgrid testbed has also be constructed to allow students to validate their controller designs. This design project has been integrated into EE5702-Advanced Power Systems Analysis module at NUS and was offered to students in August 2020. Student feedback indicates that the graduate students indeed appreciated such a hands-on experience. These findings will be published as an education paper in the near future.

**5. The Contribution, Impact or Benefit**

This research contributes to the development of the future electric grid in the presence of renewable generation and consumer dynamics. The project outcomes have been verified in both simulation and hardware, demonstrating the superiority of the proposed models/control schemes over conventional approaches. These findings would impact the design of future HDB apartments in Singapore through better integration of renewable generations and energy management of their residential loads, through the use of the microgrid configuration. As such, our studies indicate that the diversity of the Singaporean HDB residential community is a vital yet untapped resource in tackling grid operational issues by offering demand flexibility, e.g., through the control of residential home appliances and/or electric vehicles.

Dissemination of findings: Internationally, the project findings have been published in reputable scientific journals and contribute to the research in the field of microgrid design, stability, and resilience. The PI presented the findings through a research webinar to the faculty and students of the National Institute of Technology, Silchar, India in September 2020; this webinar was viewed online by over 1,000 attendees. Notably, a tutorial session on microgrid management will be delivered at the upcoming IEEE ECCE conference 2021, which is the premier conference of IEEE Industrial Applications Society.

Education: Additionally, resulting from this project, a design project has been developed to educate and train engineers about residential microgrid operation. The project has been added to the curricula of a graduate module at NUS, and was offered to students in Fall 2020. Outcomes from this course will be published as an education paper in the near future. Apart from training Singaporean engineers to fill this future market need, the project has also contributed towards raising public awareness by making lecture slides and video recordings publicly available online.

Collaborative opportunities: Overall, the project has led to several collaboration opportunities with power engineers and computer scientists from top-tier universities. For example, the research related to identifying the stable operating regions of microgrids was performed in collaboration with MIT, while the work on demand response and energy management was a joint outcome with Humboldt Universität Berlin. These collaborative efforts established future opportunities for information and research exchange as well.

**6. References to Corroborate the Contribution, Impact or Benefit**

The following is a list of contacts who have been influenced by the research outcomes:

1. Prof. James L Kirtley, MIT, USA
2. Prof. Matthias Weidlich, HU Berlin, Germany
3. Prof. Frede Blaabjerg, Aalborg University, Denmark
4. Prof. Hatem Zeineldin, Khalifa University, UAE
5. Prof. MA Asha Rani, NIT Silchar, India
6. Prof. Weidong Xiao, University of Sydney, Australia

**7. Future Plans**

The research deliverables have introduced new ways of energy management in community grids, specifically, decentralised power management strategies and baseline modelling techniques considering consumer behaviour. This additional consumer participation also opens up a possibility that consumer behaviour could be *manipulated* in power grids, thereby serving as a novel attack vector. Therefore, research/development in grid resiliency is recommended as an important future research area arising from this project.